IEEE Access
Multidisciplinary | Rapid Review | Open Access Journal

Received September 20, 2020, accepted October 11, 2020, date of publication October 19, 2020,
date of current version November 13, 2020.

Digital Object Identifier 10.1109/ACCESS.2020.3031934

NeuroFuzzy Wavelet Based Auxiliary Damping Controls for STATCOM

SAAD DILSHAD[1], (Graduate Student Member, IEEE), NAEEM ABAS[2], (Member, IEEE), HAROON FAROOQ[3], (Member, IEEE), ALI RAZA KALAIR[4], AND AWAIS AHMED MEMON[2]

[1]Department of Electrical and Computer Engineering, COMSATS University Islamabad, Islamabad 45550, Pakistan
[2]Department of Electrical Engineering, University of Gujrat, Hafiz Hayat Campus, Gujrat 50700, Pakistan
[3]Department of Electrical Engineering (RCET), University of Engineering & Technology at Lahore, Lahore 39161, Pakistan
[4]Department of Telecommunications, Electrical, Robotics and Biomedical Engineering, Swinburne University, Melbourne, VIC 3122, Australia

Corresponding author: Naeem Abas (naeemkalair@uog.edu.pk)

ABSTRACT The integration of renewable energy sources and varying load demands have risen reliability and stability issues that need proper attention and optimum solution. Continuous and reliable operation of the power system is the key to any country's economic and industrial growth. In this regard, a Static synchronous compensator (STATCOM) has extensively adapted Flexible Alternating Current Transmission System (FACTS) device mainly for Volt Ampere Reactive (VAR) compensation, voltage stability, damping oscillations to improve power system stability. In this work, A NeuroFuzzy wavelets based auxiliary control for STATCOM in a two-area power system is proposed in this article. The proposed control system was tested on four different fault scenarios. A modified Takagi-Sugeno-Kang (TSK) controller by applying a Wavelet Neural Network (WNN) is used to evaluate controllers' performance. The conventional TSK control is used to assess the performance of the proposed controllers. The TSK controller is modified by applying a WNN in the consequent part. The updated parameters in Morlet and Mexican hat wavelets are updated in the WNN, and these proposed adaptive controllers are employed as damping controllers with STATCOM. Simulation results show sufficient performance enhancement using the modified WNN based control schemes. The dynamic performance improvement is demonstrated with graphical time-domain and performance indices results using MATLAB/Simulink.

INDEX TERMS Power system stability, low-frequency oscillations, adaptive NeuroFuzzy, FACTS, Mexican Hat, morlet, power system, STATCOM.

I. INTRODUCTION

Climate change and the growing population have increased power demands and energy needs. Power systems around the world are mainly affected by industrialization, changing climate, and rapid renewable energy integration. Some developing countries are barely attaining their demands for electricity. The rapid integration of renewable energy is causing some problems related to power system operation like power quality concerns, low inertia of Photovoltaic (PV) systems, harmonics, and subsynchronous oscillations, etc. [1]. Hence, a reliable and protected operation of the power system is needed to tackle the contingencies and power surges. Low frequency oscillations are originated when power systems are subjected to any fault [2]. These oscillations, once started in a power system must need to be damped; otherwise, they grow over time and cause a cascade blackout.

There are many blackout incidents and cascade failure of power system worldwide, but the reason behind many incidents has not been studied deeply. In recent years, many countries have also reported such incidents caused due to power system stability issues. Some of them are presented in Figure 1 [3]. The reason behind some blackout is supply and demand collapse. However, Italy and US blackouts were investigated due to oscillations.

Power System Stabilizers (PSSs) have been used in the past to overcome this problem. However, PSSs are installed and controlled locally. Therefore, they fail to stabilize the power system under varying operating conditions [4]. The use of Flexible Alternating Current Transmission Systems (FACTS) controllers and energy storage devices is a crucial reason behind the centralized nature of electrical power and

The associate editor coordinating the review of this manuscript and approving it for publication was Xiaochun Cheng.

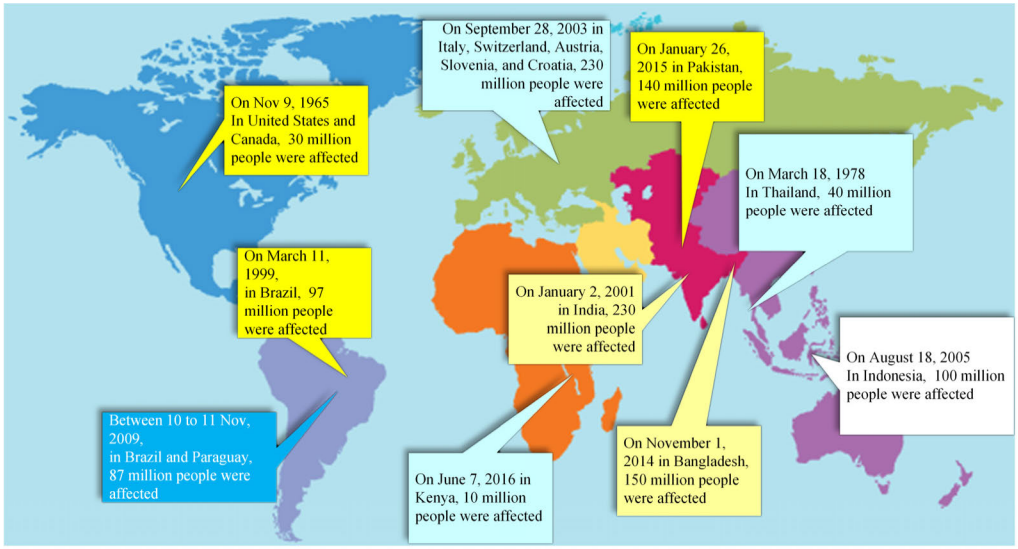

FIGURE 1. Some major power outages caused by power system instability [3].

continuously varying load demand [5]. FACTS controllers efficiently use full transmission capability and maintain the system's reliability due to their capability to improve power quality with dynamic voltage restorer (DVR) [6]. FACTS, along with an auxiliary control, can be used to damp out the low frequency oscillations effectively. Due to their fast response, FACTS devices are used to enhance steady-state performance and dynamic stability [7]. Among all other FACTS controllers, Static synchronous compensator (STATCOM) is used for power flow control, voltage control, Volt Ampere Reactive (VAR) compensation, damping oscillations, and voltage stability at long-distance transmission lines. It is also utilized for power quality improvement as Distribution STATCOM (D-STATCOM). STATCOM works in an inductive and capacitive mode by controlling its output current [8].

The control of STATCOM consists of two control loops, internal control and external control. The gating pulses for voltage source converter (VSC) are generated by internal control. The external control, known as Auxiliary Damping Control (ADC), is used to adjust the internal control parameters to damp the oscillations in the power system.

The rest of the paper is constructed as; the literature review for power system stability enhancement using STATCOM, and applications of NeuroFuzzy controllers have been presented in the next section. The ADC mechanism, introduction of neural network and fuzzy system, detailed layer structure of NFWC and its self-tuning algorithm are presented in section III; the simulation results are presented and discussed in the graphical and quantitative results section, and in last, a conclusion is presented with a focus on the key findings of this work.

II. LITERATURE REVIEW

In literature, different control schemes have been proposed and adapted for power oscillations damping with STATCOM. The proposed techniques involve Proportional Integral [9], swarm and bat algorithm [10], Harmony Search Evolutionary (HSE) technique [11], and Imperialist Competitive Algorithm (ICA) [12], etc. However, some of these linear and nonlinear techniques lack in adapting the system uncertainties and fail to retain performance under different contingencies [13]. In recent years, damping of power system oscillations for nonlinear and dynamic plants has been achieved using NeuroFuzzy control techniques with STATCOM [14]–[16]. But most of these techniques incorporate Takagi-Sugeno-Kang (TSK) structure with a linear consequent part that cannot effectively transform the system uncertainties and nonlinearities into NeuroFuzzy control, as new technology, fuzzy Wavelet Neural Network (WNN), was introduced, which integrates conventional TSK structure with wavelets.

Neural Network (NN) has attributes of learning capability, nonlinear mapping, and highly interconnected parallel network. However, NN requires a large number of neurons for solving complex approximation problems, and NN may be stuck in the local minimum due to the non-convexity of the error function in the neural network. The use of wavelet function in the network can overcome these disadvantages of the neural network.

The fuzzy system reduces the complexity of data and can model uncertainties. NN have learning capability, and wavelets have localized property to discover the detail of non-stationary signals. This combination allows developing a system with the ability to specify a nonlinear system that can learn quickly [17], [18]. Fuzzy wavelet neural networks have been used to control nonlinear and dynamic plants successfully [17]. Proper initialization of parameters is required for fast convergence in wavelet neural networks. For the increased speed and fast convergence, optimum values of translation and dilation parameters are used [19].

Due to the earlier mentioned capabilities of NeuroFuzzy wavelet control, it is used in a wide variety of applications from the prediction of electricity consumption and time series [20], [21], to use in robot manipulators [22], vehicle suspension control [23], power system stabilizer design [24], SSSC based power oscillation damping [25], and long-term load forecasting, [19] etc.

This article presents a direct adaptive NeuroFuzzy control method using a WNN. The proposed control paradigm uses antecedent parts of conventional TSK and Morlet and Mexican hat wavelets based WNN in the TSK controller's consequent part. The use of Wavelets in the consequent part improves the computational power of the neuro-fuzzy system.

The main contributions of this research work are summarized below:

- to demonstrate a systematic procedure of direct adaptive NeuroFuzzy Wavelet Control (NFWC) strategy employing Morlet and Mexican hat wavelets for the design of an ADC for STATCOM.
- to validate the proposed control strategy by analyzing the performance of NFWC (Morlet) and NFWC (Mexican hat) controls with a conventional TSK control under different symmetric and unsymmetrical faults scenarios.
- to demonstrate performance improvement by assessing various Performance Indices (PIs).

The modeling aspect of the synchronous machine and power system with STATCOM are not addressed in this article, with a prime focus on the controller implementation with STATCOM. The synchronous machine model having d axis lagging the q axis is presented in [26], [27]. and the detailed power system model for STATCOM with multimachine power system can be found in [13].

III. AUXILIARY DAMPING CONTROL MECHANISM

The output current of the STATCOM is controlled by incorporating three different ADC schemes in this work. These ADC acts as damping controllers for power oscillations when installed with STATCOM. The ADC compared in this work are Adaptive NeuroFuzzy TSK Control (ANFTskC), Adaptive NeuroFuzzy Morlet Wavelet Control (ANFMoWC), and Adaptive NeuroFuzzy Mexican hat Wavelet Control (ANFMhWC). A closed-loop system involving the ADC mechanism connected to a plant is shown in Figure 2.

A two-area power system having two machines with STATCOM already installed is used as a plant in this work. The rotor speed deviation between both machines is used as plant output and fed to the controller. The input to the NeuroFuzzy ADC is $(\Delta\omega_r - \Delta\omega_{21})$ and its derivative. Where, $\Delta\omega_r$ is reference deviation and $\Delta\omega_{21}$ is the actual rotor speed deviation between two machines. The ADC block gives the output as; $u \in \{u_{\text{ANFMoWC}}\ u_{\text{ANFMhWC}}\ u_{Tsk}\}$ for ANFMoWC, ANFMhWC, and ANFTskC, respectively.

This output is modulated with a reference voltage and supplied to internal control of STATCOM. A detailed, layered

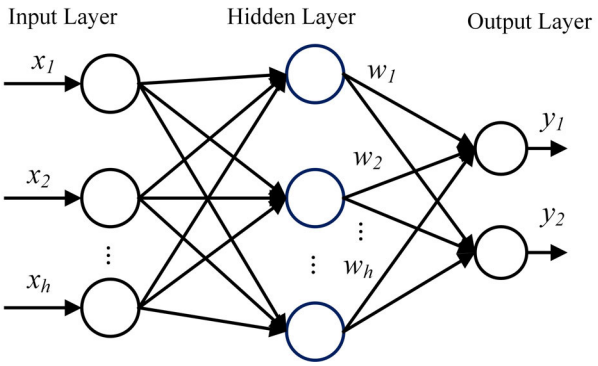

FIGURE 2. Closed-loop system.

structure of the proposed controllers is given in the following subsection.

A. NEURAL NETWORK AND FUZZY SYSTEM

NN consists of a number of simple and highly interconnected processing elements operating in parallel. This network is inspired by the biological nervous system. The structure of the NN consists of perceptron and synaptic connections. The processing elements perceptron (neuron) are connected through other neurons with the connections called synapses. In simple NN, the synapses' influence is included with connection weight, which regulates the influence of the corresponding input signal. The drawback of the neural network is an intricate design structure and black-box nature of its operation. The structure of the NN is shown in Figure 3.

Lofti Zadeh first introduced the fuzzy set theory in 1965 [28]. Fuzzy systems use mathematics to translate human knowledge into artificial intelligence. Fuzzy systems are described with the help of fuzzy rules which use a linguistic term such called rules; IF $<$ antecedent $>$ THEN $<$ consequent $>$. Fuzzy quantities are described in terms of fuzzy sets or fuzzy numbers. Fuzzy systems are very efficient at approximating real continuous functions to a high degree of accuracy.

Figure 4 shows a simple fuzzy logic system consisting of three stages. The first stage is called fuzzification, in which inputs are fuzzified by mapping a function. In the second stage, the membership values estimated in the fuzzification block are aggregated to get a single degree of membership. This process is done in the fuzzy inference, which uses a fuzzy rule base to perform the decision-making process. In the last stage, the resulting fuzzy values are converted back to numerical or crisp values. This process is called defuzzification.

The fuzzy system processes the rules in accordance with the firing strength of the inputs. This is performed by fuzzy operators like conjunction (AND), dis-junction (OR), and complement (NOR) operator. In the last stage, the fuzzy system is transformed again into crisp space; this process is called defuzzification. The mathematical model which uses fuzzy sets is known as fuzzy models. The two types of

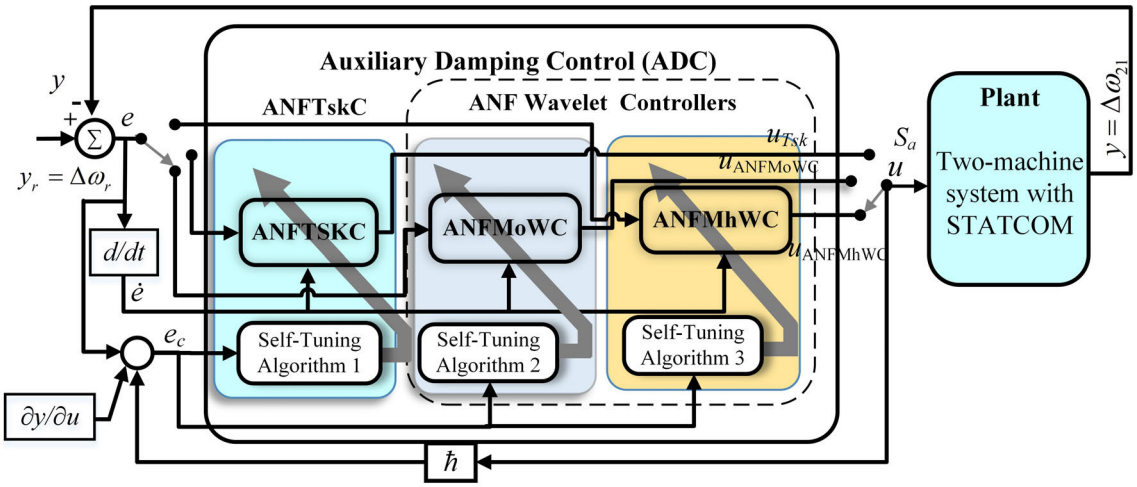

FIGURE 3. Structure of Neural Network.

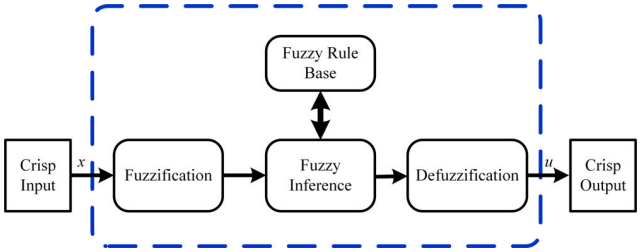

FIGURE 4. Fuzzy logic system.

fuzzy models Mamdani and TSK, are widely used in the literature [29].

NeuroFuzzy is the fusion of a Fuzzy Inference System (FIS) and Artificial NN (ANN). NeuroFuzzy systems have gained widespread interest for the researchers in engineering and other scientific areas due to the need for adaptive intelligent systems to solve real-world problems. FIS specifies the fuzzy sets, fuzzy operator, and knowledge base, and ANN stipulates the architecture and learning algorithm. The approaches to integrate the FIS and ANN can be broadly classified into three categories; cooperative model, concurrent model, and fully fused model.

B. LAYARD STRUCTURE OF ADAPTIVE NEUROFUZZY WAVELET CONTROL

In the proposed control scheme, the conventional TSK controller's consequent part is substituted with a WNN. The layered architecture for ANFTskC is presented in Figure 5. It consists of 6 layers, the first two layers belong to the antecedent part, and Layer 3 belongs to the consequent part. A linear polynomial is used in the consequent part of ANFTskC, and WNN is incorporated in it for proposed controllers. Fuzzy rules interconnect this multi-layer NN. The circle and square indicate a fixed node, and the rectangle indicates an adaptive node of the antecedent and consequent section.

The general rule for the ANFWC is described by:

$$\mathrm{R}_j : \mathrm{IF}\ x_1 \text{ is } \mathrm{E}_{1j} \quad \text{and} \quad x_2 \text{ is } \mathrm{E}_{2j} \text{ and } \cdots x_h \text{ is } \mathrm{E}_{hg}$$
$$\mathrm{THEN} \kappa_j = w_j \sum_{i=1}^{h} \Lambda_j (x_i) \tag{1}$$

Here $x_1, x_2, \ldots, x_h$ are crisp inputs and E_{ij} is the membership function for ith input and jth rule. κ_j is a the jth output of the WNN. In case of ANFTskC, the κ_j is given as linear function as;

$$\kappa_j = \sum_{i=0,i=1}^{h,g} b_{ij} x_i \quad where\ x_0 = 1 \tag{2}$$

Layer 1 contains the membership function. The membership degree to the fuzzy set for each input set is determined here.

The Gaussian membership is expressed as:

$$\mathrm{E}_{ij} = \exp\left(-\frac{1}{2}\frac{(x_i - \chi_{ij})^2}{\delta_{ij}^2}\right) \quad i = 1, 2, \ldots, h, j = 1, 2, \ldots, g \tag{3}$$

here, δ and χ are the standard deviation (STD) and mean of the membership function.

In layer 2, the number of nodes corresponds to the number of rules. The output of each node represents the firing strength of each rule, and And (min) operator calculates the output in this layer.

The expression for layer 2 is given as

$$\mathrm{B}_j = T\left[\mathrm{E}_1\, \mathrm{E}_2 \mathrm{E}_3 \ldots \mathrm{E}_g\right] \tag{4}$$

where, B_J gives the firing strengths of each rule calculated by triangular norm product operation. The E_{ij} denotes the Gaussian membership function.

The key design of ANFTskC, ANFMoWC, and ANFMhWC vary in the consequent part. The architecture of both proposed controllers having WNN is illustrated in Figure 6. The wavelets are incorporating in the form of WNN. The neural network has limited ability to characterize the

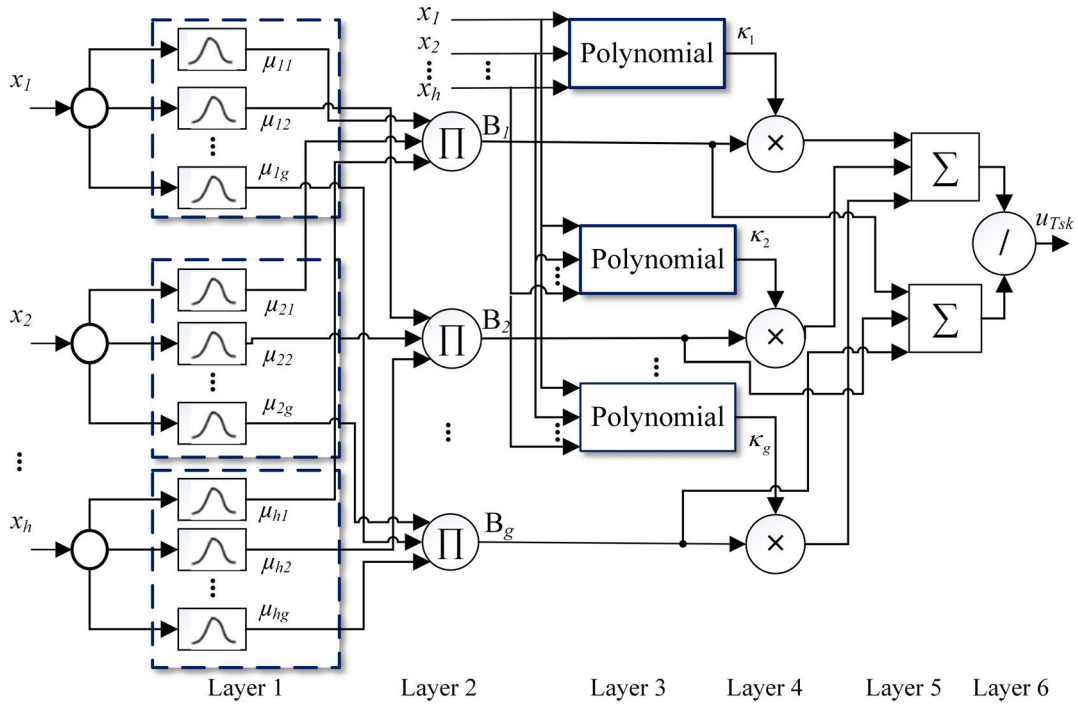

FIGURE 5. Layers structure of ANFTskC.

local features of the time series. The use of wavelet function in the system can overcome these disadvantages of the neural network. The parameters of the wavelets and weights between the hidden and output layers are also adapted in each iteration. The ANFTskC consists of a linear function given in (2) [30], and the output of layer 3 comprising a WNN is given as;

$$\kappa_j = w_j \sum_{i=1}^{h} \Lambda_j (x_i) \tag{5}$$

Here, $\Lambda_j (x_i)$ denotes wavelet function and Morlet wavelet (Mo) and Mexican hat wavelet (Mh) are expressed in (6) and (7), respectively:

$$\Lambda_j(x_i)_{\text{Mo}} = \cos(5\sigma_{ij}) e^{-0.5\sigma_{ij}^2} \tag{6}$$

$$\Lambda_j(x_i)_{\text{Mh}} = \sum\nolimits_{i=1}^{h} |\alpha|^{-0.5} \left(1 - \varsigma_{ij}^2\right) e^{-0.5\varsigma_{ij}^2} \tag{7}$$

where,

$$\sigma_{ij} = \left[\frac{x_i - \beta 1_{ij}}{\alpha 1_{ij}}\right] \quad \text{and} \quad \varsigma_{ij} = \left[\frac{x_i - \beta 2_{ij}}{\alpha 2_{ij}}\right] \tag{8}$$

Here, αk_{ij} and βk_{ij} are the dilation and translation parameters, respectively, and k = 1 and 2, which distinguish between Morlet and Mexican hat wavelet. The structure of the WNN is shown in Layer 3 of Figure 6. It has three layers: an input layer, a hidden layer, and an output layer. The neurons in the hidden layer are also called *wavelons*.

The Morlet and Mexican hat wavelet functions are presented in Figure 7. These wavelets were used to replace the linear polynomial in the ANFTskC, and new controllers were formed with adaptive weights, dilation, and translation parameters to enhance the performance of the ANFTskC.

In layer 4, The output of the antecedent part and WNN is multiplied, and the process of defuzzification is completed in the next layers [31];

$$u = \frac{\sum_{j=1}^{g} \text{B}_j \kappa_j}{\sum_{j=1}^{g} \text{B}_j} \tag{9}$$

Here, the outputs for each controller is given in the set $u \in \left\{ u_{Tsk} \; u_{\text{ANFMoWC}} \; u_{\text{ANFMhWC}} \right\}$.

The number of updated parameters in the conventional adaptive controller (TSK) and proposed controllers are given in Table 1.

C. SELF-TUNING ALGORITHM

The self-tuning algorithm is required to update the antecedent and the consequent parameters of the proposed controllers. The parameters presented in Table 1 are updated in every iteration by updating with gradient descent based algorithm. The following cost function is minimized to update the controller parameters;

$$\text{X} = 0.5 \left[(y_r - y)^2 + \text{h}u^2 \right] \tag{10}$$

Here, $y_r = \Delta\omega_r$ is the reference speed deviation and $y = \Delta\omega_{21}$ is the actual speed deviation of plant in this work, respectively. '$\hbar$' is the a constant term and 'u' is the output

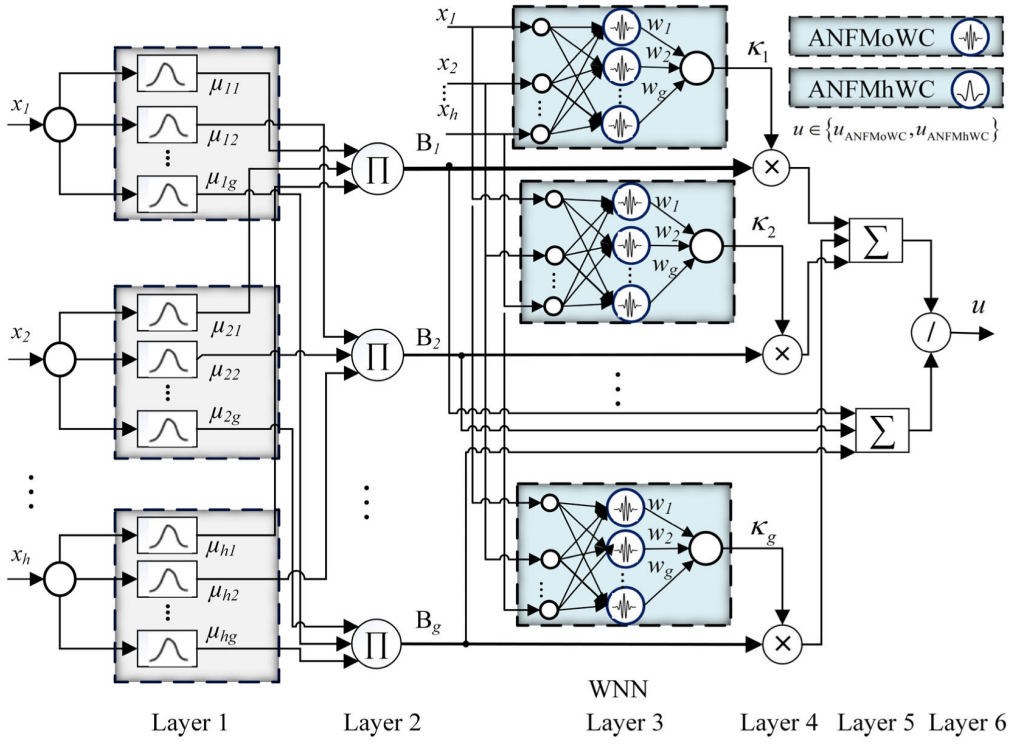

FIGURE 6. Layers structure of ANFWC (ANFMoWC and ANFMhWC).

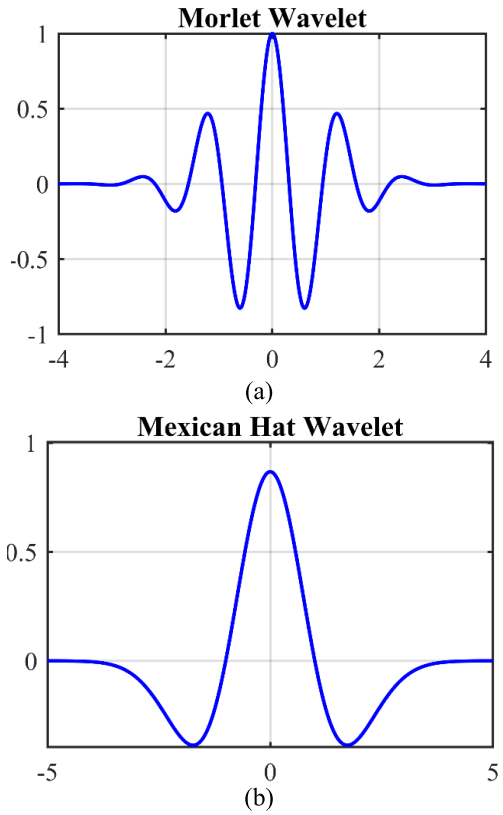

FIGURE 7. (a) Morlet wavelet (b) Mexican hat wavelet.

of the controller and expressed for adaptive controllers as $u \in \{u_{Tsk}\ u_{\text{ANFMoWC}}\ u_{\text{ANFMhWC}}\}$.

TABLE 1. Update parameters comparison (TSK, ANFMoWC, ANFMhWC).

Control scheme Controller Parameters	ANFTskC	ANFMoWC	ANFMhWC
Antecedent part (Mean and STD)	(δ_{ij}, χ_{ij}) 8	(δ_{ij}, χ_{ij}) 8	(δ_{ij}, χ_{ij}) 8
Consequent part	Linear Polynomial b_{ij} 6	Morlet Wavelet $\alpha 1_{ij}$ and $\beta 1_{ij}$ 6	Mexican Hat Wavelet $\alpha 2_{ij}$ and $\beta 2_{ij}$ 6
Weights (w_j)	0	2	2
Total Update Parameters	**14**	**16**	**16**

No prior training data is required in proposed adaptive controllers, and parameters are trained online without any training data. Therefore, these controllers are also known as online adaptive controllers. The most adapted rule for training NN is the Back Propagation algorithm (BP). The BP algorithm is based on gradient descent optimization. The network can converge to the desired value by applying the BP learning algorithm to adjust the weights of the ANNs by reducing the accumulated mean square error. BP utilizes the derivative of the error in each iteration. The overall parameters of the network are adjusted using a gradient descent based BP algorithm.

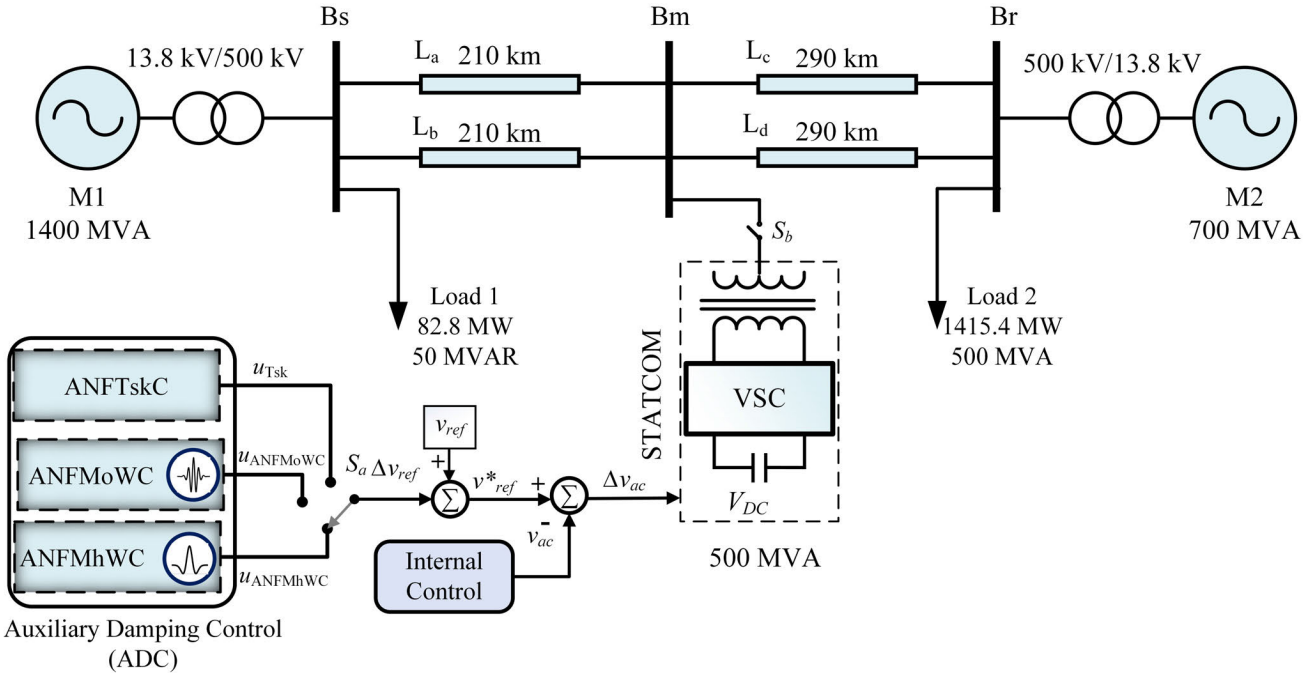

FIGURE 8. Single line diagram showing a two-area test system with ADC based STATCOM.

The steepest-decent based update rule is used to update the parameters;

$$C(t+1) = C(t) - \lambda \frac{\partial \mathrm{X}}{\partial C} + \mathrm{D}(C(t) - C(t-1)) \quad (11)$$

Here, $C = \left[\delta_{ij}, \chi_{ij}, \alpha 1_{ij}, \alpha 2_{ij}, \beta 1_{ij}, \beta 2_{ij}, w_j\right]$ consists of all the update parameters of the ANFMoWC and ANFMhWC based networks. λ and D are the learning rate and momentum term, respectively. Momentum term is used to speed up the convergence, and it is only used in consequent parameters here. The momentum term is zero for STD and mean parameters.

The parameters of antecedent part are updated using following rule.

$$C_A(t+1) = C_A(t) - \frac{\partial \mathrm{X}}{\partial C_A} \quad (12)$$

Here, $C_A = \left[\delta_{ij}, \chi_{ij}\right]$ consists of only mean and STD parameters of the proposed controllers. The partial derivative in (12) is derived using the following chain rules.

$$\frac{\partial \mathrm{X}}{\partial \delta_{ij}} = \sum_j \Gamma \left[\frac{\partial u}{\partial B_J} \frac{\partial B_J}{\partial \mathrm{E}_{ij}} \frac{\partial \mathrm{E}_{ij}}{\partial \delta_{ij}}\right] \quad (13)$$

$$\frac{\partial \mathrm{X}}{\partial \chi_{ij}} = \sum_j \Gamma \left[\frac{\partial u}{\partial B_J} \frac{\partial B_J}{\partial \mathrm{E}_{ij}} \frac{\partial \mathrm{E}_{ij}}{\partial \chi_{ij}}\right] \quad (14)$$

where, $\Gamma = \left[\frac{\partial \mathrm{X}}{\partial y} \frac{\partial y}{\partial u} + \hbar u\right]$, the final update equations are derived by combining (13), (14) and (11) into (12). The term $\partial y / \partial u$ is also called plant sensitivity measure, and in direct adaptive control this term is kept constant [32].

The design variation between ANFTskC, ANFMoWC, and ANFMhWC lies in the consequent part of the network. Therefore, the update rule for deriving the dilation and translation parameters for Morlet and Mexican hat wavelet is given as;

$$C_C(t+1) = C_C(t) - \frac{\partial \mathrm{X}}{\partial C_C} + D(C_C(t) - C_C(t-1)) \quad (15)$$

Here, $C_C = \left[\alpha 1_{ij}, \alpha 2_{ij}, \beta 1_{ij}, \beta 2_{ij}, w_j\right]$, and D momentum term is only used in consequent part to speed up the convergence of the WNN.

The partial derivative in WNN of ANFMoWC control in (15) are derived as:

$$\frac{\partial \mathrm{X}}{\partial \alpha 1_{ij}} = \Gamma \left[\frac{\partial u}{\partial \kappa_j} \frac{\partial \kappa_j}{\partial \Lambda_{j\mathrm{Mo}}} \frac{\partial \Lambda_{j\mathrm{Mo}}}{\partial \sigma_{ij}} \frac{\partial \sigma_{ij}}{\partial \alpha 1_{ij}}\right] \quad (16)$$

$$\frac{\partial \mathrm{X}}{\partial \beta 1_{ij}} = \Gamma \left[\frac{\partial u}{\partial \kappa_j} \frac{\partial \kappa_j}{\partial \Lambda_{j\mathrm{Mo}}} \frac{\partial \Lambda_{j\mathrm{Mo}}}{\partial \sigma_{ij}} \frac{\partial \sigma_{ij}}{\partial \beta 1_{ij}}\right] \quad (17)$$

Similarly, for WNN of ANFMhWC control:

$$\frac{\partial \mathrm{X}}{\partial \alpha 2_{ij}} = \Gamma \left[\frac{\partial u}{\partial \kappa_j} \frac{\partial \kappa_j}{\partial \Lambda_{j\mathrm{Mh}}} \frac{\partial \Lambda_{j\mathrm{Mh}}}{\partial \varsigma_{ij}} \frac{\partial \varsigma_{ij}}{\partial \alpha 2_{ij}}\right] \quad (18)$$

$$\frac{\partial \mathrm{X}}{\partial \beta 2_{ij}} = \Gamma \left[\frac{\partial u}{\partial \kappa_j} \frac{\partial \kappa_j}{\partial \Lambda_{j\mathrm{Mh}}} \frac{\partial \Lambda_{j\mathrm{Mh}}}{\partial \xi_{ij}} \frac{\partial \sigma_{ij}}{\partial \beta 2_{ij}}\right] \quad (19)$$

The partial derivative for weights is calculated as:

$$\frac{\partial K}{\partial w_j} = \Gamma \frac{\partial u}{\partial \kappa_j} \frac{\partial \kappa_j}{\partial w_j} \quad (20)$$

Using (16) to (20) and (11) into (15), the complete update law is formed which is used for adaptation of these update parameters.

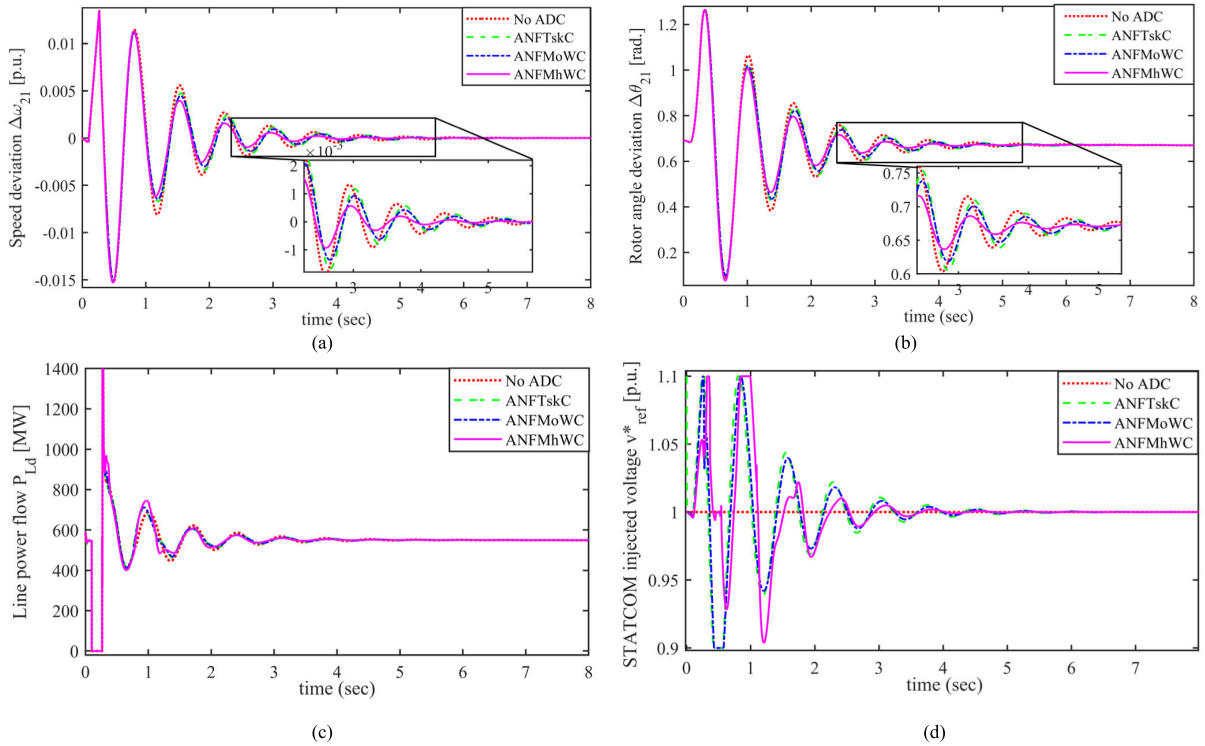

FIGURE 9. Case -1: (a) Speed deviation ($\Delta\omega_{21}$) (b) Angle deviation ($\Delta\theta_{21}$) (c) Line power flow (P_{Ld}) (d) Injected voltage in STATCOM (v^*_{ref}).

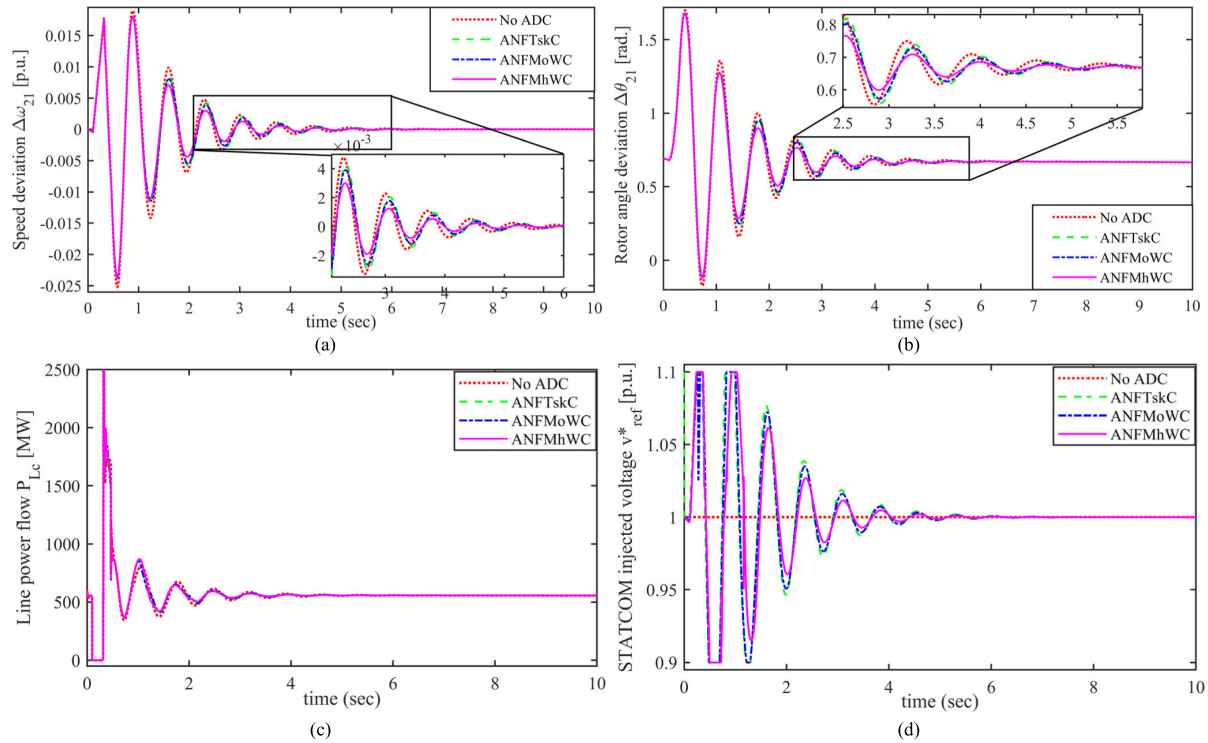

FIGURE 10. Case -1: (a) Speed deviation ($\Delta\omega_{21}$) (b) Angle deviation ($\Delta\theta_{21}$) (c) Line power flow (P_{Ld})(d) Injected voltage in STATCOM (v^*_{ref}).

IV. GRAPHICAL AND QUANTITATIVE RESULTS

A simulation study was performed on a Core i5 5th generation computer with 8 GB of installed memory on MATLAB/Simulink platform. A STATCOM connected to a two-machine system is employed in this work with machine ratings of 1400MVA and 700 MVA, for G1 and

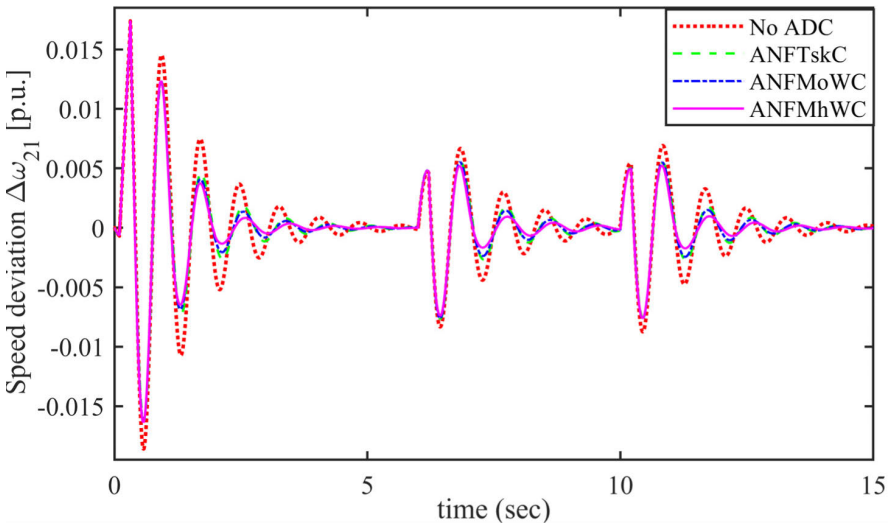

(a)

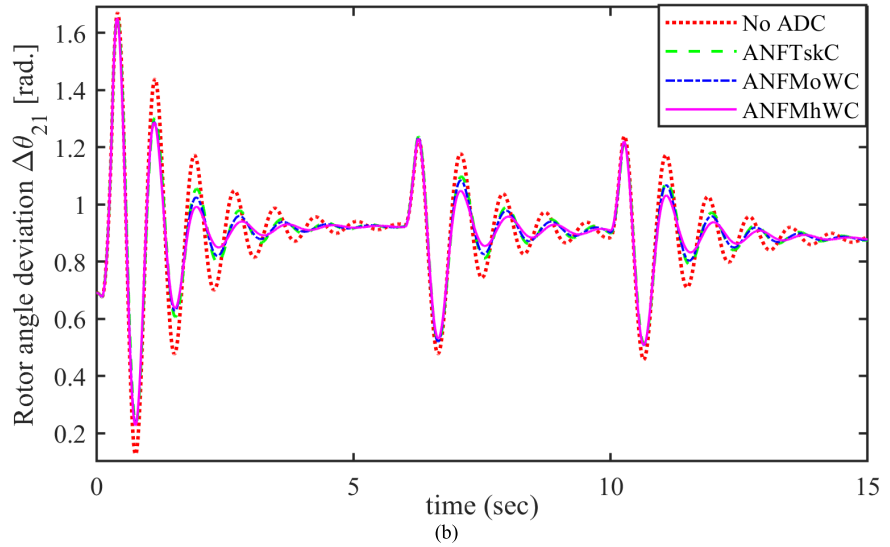

(b)

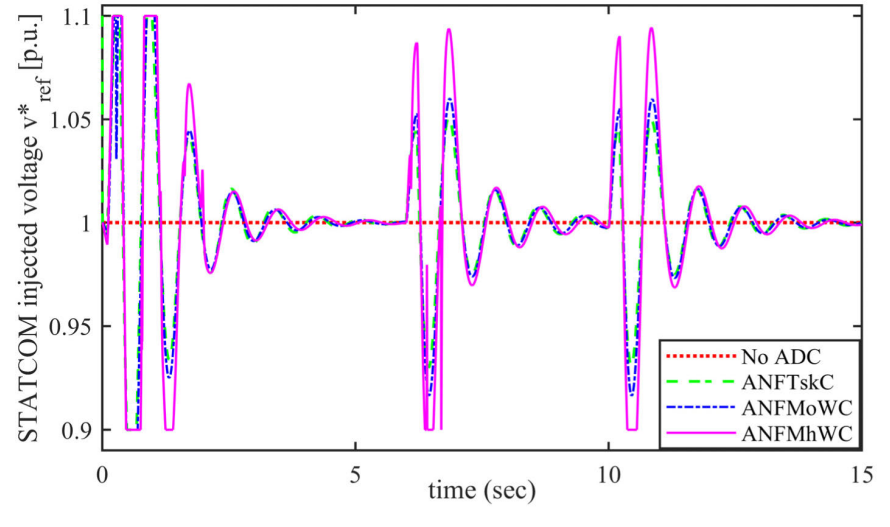

(c)

FIGURE 11. Case -3: (a) Speed deviation ($\Delta\omega_{21}$) (b) Angle deviation ($\Delta\theta_{21}$) (c) Injected voltage in STATCOM (v^*_{ref}).

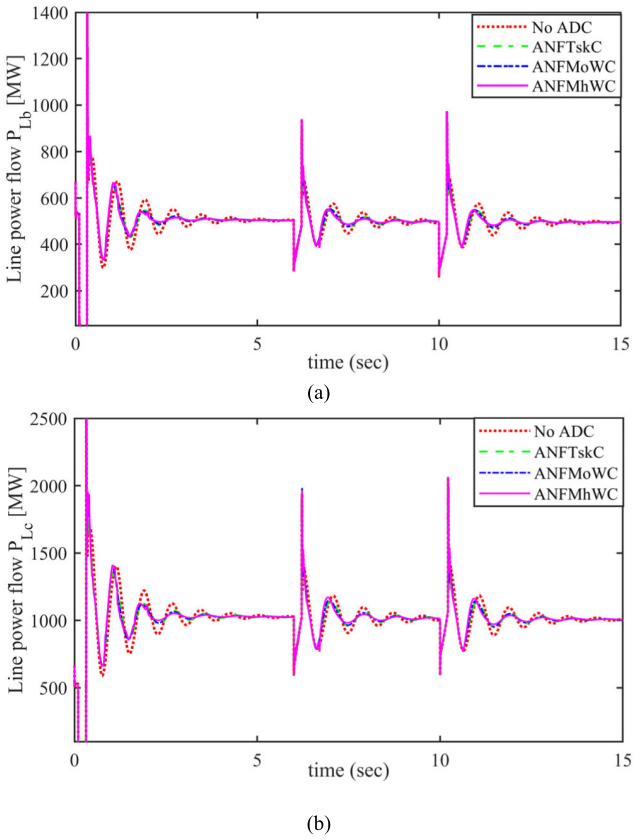

FIGURE 12. Case-3: (a) Line power flow (P_{Lb}) (b) (a) Line power flow (P_{Lc}).

G2, respectively. The two machines are connected to the step-up transformer and transmission lines. The length of transmission lines is 210 km for L_a and L_b, and 290 km for L_c and L_d. A 500 MVA STATCOM is installed at Bus m (Bm). In stability studies, a slightly off-centered location is suggested for the installation of STATCOM in [33].

The generators are equipped with PSS, and simulations are performed without disturbing the machine's existing PSS controls. The other parameters of the power system are shown on the single line diagram in Figure 8. The simulation study was performed for four different contingency conditions involving three-phase fault, line outages, the line to line faults, and line to ground faults in different cases. The switch S_a depicts the test scenario of the power system with ANFMoWC, ANFMhWC, and ANFTskC. The switch S_a remains open when STATCOM is used without any ADC. The switch S_b can used to connect and disconnect STATCOM with test system.

A. CASE 1

A three-phase self-clearing fault was applied on receiving end side at line L_c. The fault starts at t = 0.1 sec and remains for only ten cycles and then cleared from the system. Figure 7 (a) and (b) shows the rotor speed and angle deviations. The ANFMhWC has shown better damping of speed deviation and brings the system in a steady state before the other controllers do. The oscillations in rotor speed and angle are more significant for STATCOM without ADC. The amplitude of rotor angle oscillations is less for ANFMhWC than ANFMoWC, ANFTskC, and STATCOM without ADC. Marginal performance enhancement is seen between ANFMhWC and ANFMoWC, as both of these controls are having WNN in the consequent part. The power flow on L_d is shown in Figure 9 (c). The power flow is disturbed during the fault duration, and in a stable state, it reaches approximately 550 MW. Figure 9 (d) displays the injected voltage of the STATCOM, which is modulated with its internal control, which in turn control the impact of the STATCOM on power system connected at Bm.

B. CASE 2

The test system undergoes a more stressed fault scenario, which involves rapid variations in system conditions. A three-phase fault is applied at line L_d from t = 0.1 to 0.315 sec, and another fault further evaluates the test system. Another fault of partial line outage is practiced by removing the line at t = 0. 3 to re-closure at 0.4667 sec. Figure 10 (a) and (b) shows the rotor speed and angle deviation, ANFMhWC shows significant better damping of rotor angle deviation then ANFMoWC, ANFTskC, and without ADC. The damping performance of STATCOM without ADC is poor in steady-state and transient state. The steady-state line power flow is approximately 550 MW, as shown in Figure 10 (c). The injected voltage by the STATCOM controlled by the output of the controller is exhibited in Figure 10 (d).

C. CASE 3

The robustness of the proposed control design is assessed by implementing complex faults in series, and the test system is examined with a more practical and stressed scenario. A symmetric three-phase fault is applied at line L_d at t = 0.1 to 0.315 sec. This fault is cleared by permanent removal of line L_d from the system, and power flow is halted on this line. An unsymmetrical self-clearing phase to ground fault is applied at L_a at t = 6 sec for 12 cycles, and another phase to phase fault is applied at line L_b at t = 11 sec before the system gets stabilize from the effect of the previous fault. The unsymmetrical fault remains on line L_b for ten cycles only.

Figure 11 (a) and (b) shows the rotor speed deviation and rotor angle deviation between machine 1 and 2, respectively. It depicts that the severeness of the symmetrical fault is much larger than the unsymmetrical fault as it applies to all the phases. Hence, this short circuit causes a considerable amount of deviations in both rotor speed and the angle between both machines. Results show that the ADC has played their role starting from the first swings and effectively damped the oscillations in the transient regions. The swings are low in less critical unsymmetrical faults then three-phase fault, and proposed controller ANFMhWC and ANFMoWC have shown much better damping of oscillations in all three faults. ANFMhWC has performed much efficient damping than

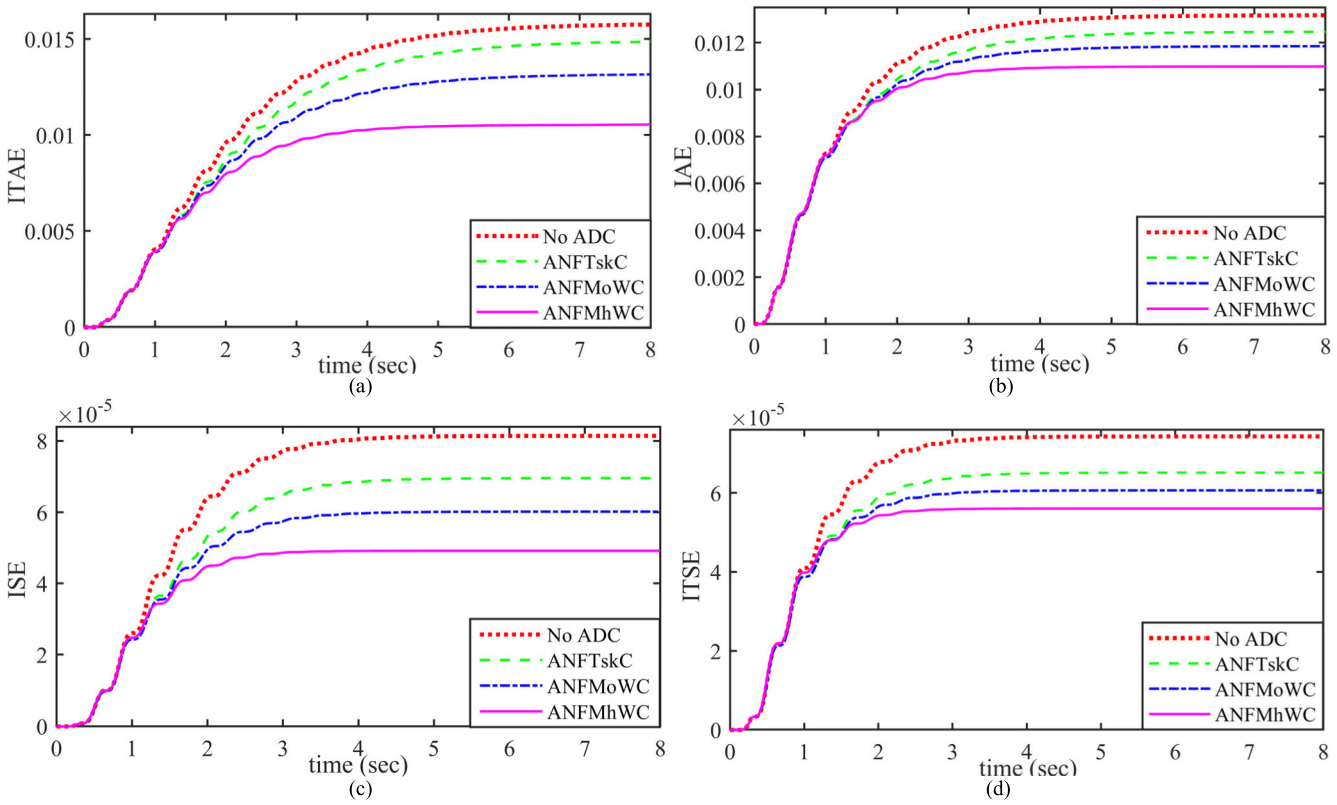

FIGURE 13. Case 1: (a) ITAE (b) IAE (c) ISE (d) ITSE.

ANFTskC; however, its performance is slightly better than the ANFMoWC.

The performance of STATCOM without ADC is inferior in three faults scenarios. The injected voltage into the internal control of STATCOM is shown in Figure 11 (c) shows that the injected voltages are almost the same in the starting time of the first fault, and after that, ANFMhWC has demonstrated higher than ANFMoWC and ANFTskC, which resulted in smooth damping of oscillations.

Figure 12 (a) and (b) shows the power flow on L_b and the only healthy line L_c of the system. The line power flow fluctuates after the fault and stabilizes at 505 MW during the steady-state condition. It shows that pre-fault power flow is 525 MW, and it increases to 1025 MW when the permanent outage clears the fault of Ld. Higher power oscillations are observed in STATCOM without ADC case in all faults scenarios.

D. PERFORMANCE EVALUATION

Describing the performance of different control schemes is a tough task; however, the nonlinear time-domain simulations tool provides visual information to analyze the performance of various proposed control techniques. It is a prime testing tool for transient stability analysis. Sometimes, performance improvement among different control paradigm is difficult to analyze because it is insignificant or marginal in both transient and steady-state regions. To get a complete sharp judgment of the system results, in the sense which can rank the performance from worst to best. The behavior of ADCs for STATCOM is analyzed by using different PIs. PIs provide help not only to insight the performance of the control system in transient and steady-state regions, but a quantitative measurement can also be drawn from these. PIs are calculated as;

$$\text{PIs} = \int_0^{t_{sim}} t^a |e(t)|^b dt \quad \textit{where a and b are constants} \tag{21}$$

The Integral Time Square Error (ITSE), Integral Time Absolute Error (ITAE), Integral Square Error (ISE), and Integral Absolute Error (IAE) are calculated using the (a, b) such as (1,2), (1,1), (0,2) and (0,1), respectively.

The PIs for two-machine test system is calculated as:

$$\text{PI} = \int_{t=0}^{t_{sim}} t^a |\omega_2 - \omega_1|^b dt \tag{22}$$

were, $|\omega_2 - \omega_1|$, represents the absolute value of the rotor speed deviations between machine 2 and machine 1.

A quantitative measure of the performance of the different control techniques has been carried out to check the overall performance improvement among controllers.

Percentage improvement is determined with the following expression [34];

$$\text{PI \% improvement for G w.r.t. H} = \frac{\text{PI}_\text{H} - \text{PI}_\text{G}}{\text{PI}_\text{H}}\% \tag{23}$$

where, G ∈ {ANFTskC, ANFMoWC, ANFMhWC} and 'H' denotes STATCOM without ADC.

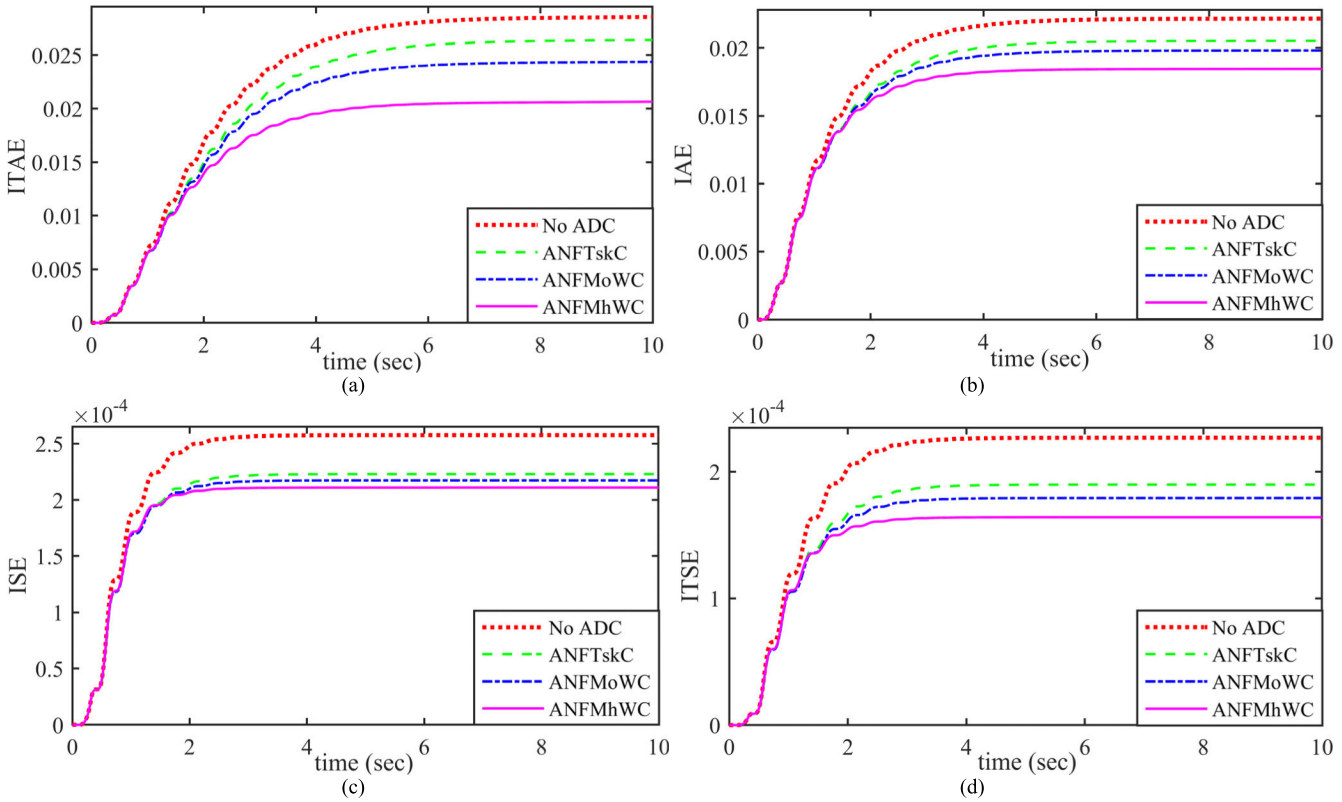

FIGURE 14. Case 2: (a) ITAE (b) IAE (c) ISE (d) ITSE.

The graphical results of PIs for case 1 are shown in Figure 13. The PIs curves show that the performance margin is more in ITAE and ISE than IAE and ISE in this case. Marginal performance enhancement is seen for ANFMoWC and ANFMhWC for IAE and ITSE, but the IAE curve shows that the transition from transient state to steady-state is sharp for ANFMhWC. ANFMhWC gives better performance all PIs curves, and the slope has become zero in steady-state and gives better results when compared to ANFMoWC, ANFTSKC, and STATCOM without ADC case. Hence, ANFMhWC and ANFMoWC have performed better in both steady-state and transient states.

The PIs curves for case 2 are shown in Figure 14. The PIs ITSE and ISE depicts the performance improvement in the transient region, and PIs without squares show a better illustration of performance during steady-state. The results show that performance improvement achieved by the proposed controller is more significant in ITSE and ITAE. The performance improvement for ANFTskC and ANFMoWC is very close for IAE and ISE, but distinct difference in performance has been observed for ANFMoWC and ANFMhWC for ITAE and ITSE. The PIs curves show the superiority of performance for ANFMhWC in all PIs. The performance of ANFMoWC and ANFMhWC is marginal when compared to each other. However, there is a significant difference observed than ANFTskC and without ADC. ANFMhWC gives better performance than ANFMoWC in steady-state and transient states.

PIs curves for case 3 are shown in Figure 15. It shows that more performance has been achieved in ITAE and IEA curves; it is by better damping of oscillations by proposed controllers in steady-state regions. Thus the robustness of the proposed controller is tested under three faults in series, and ANFMoWC and ANFMhWC have shown better performance in all three faults duration. The performance improvement for ANFTskC and ANFMoWC is very close in the first fault for ISTE, ISE, and ITAE, but after the second fault, the performance of ANFMoWC can be easily detected in PIs curves. The performance of proposed ANFMhWC and ANFMoWC is significantly better than ANFTskC and STATCOM without ADC. The ANFMhWC has shown better performance over ANFMoWC in all PIs curves.

The computation time for all the text cases with different controllers is presented in Table 2. It is clear from the computational time taken No ADC and ANFTskC are much smaller, and ANFMoWC and ANFMhWC take a longer time due to the involvement of more update parameters during each iteration. This is due to the more computation complexities involved by the inclusion of wavelets in the conventional ANFTskC. The table also depicts the speed deviation curves' peak magnitude to examine the proposed control strategy's effectiveness. It shows that at the time when a fault comes on the system, a significant swing of rotor speed deviation appears and these swings are almost same for all the case as fault was applied on 0.1 s and the first swing reaches its peak at just 0.167 s at t=0.267 and controller start working

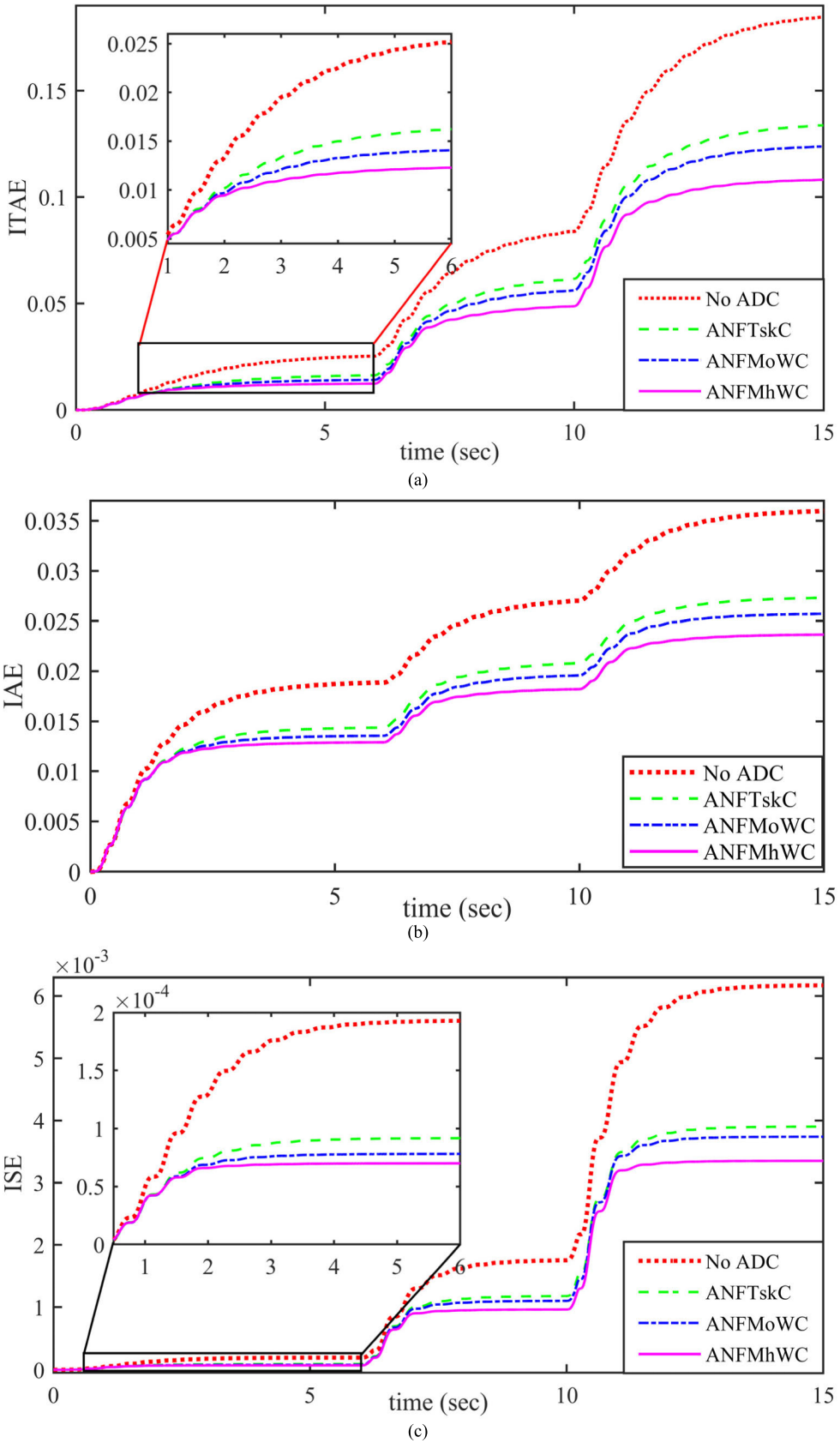

FIGURE 15. Case 3: (a) ITAE (b) IAE (c) ISE (d) ITSE.

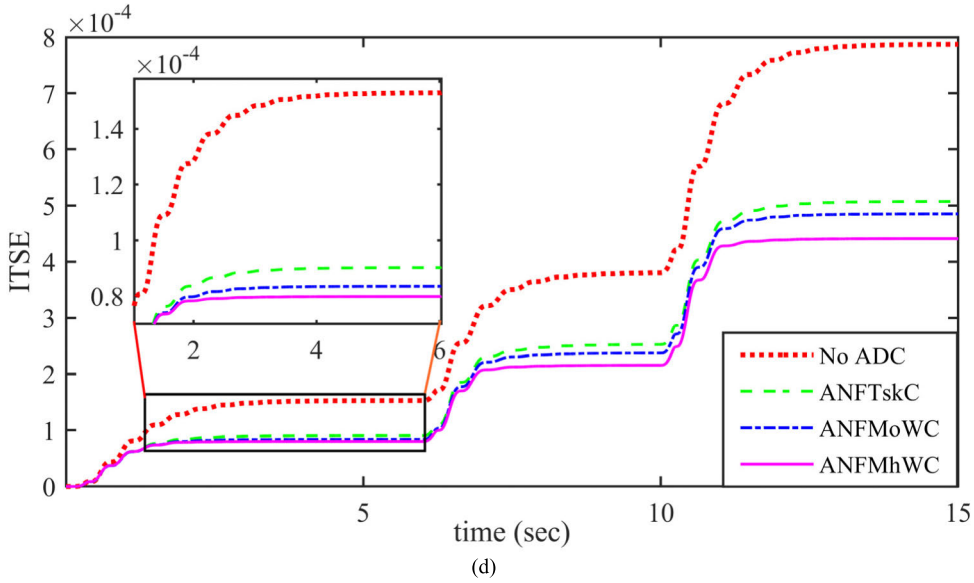

(d)

FIGURE 15. *(Continued.)* **Case 3: (a) ITAE (b) IAE (c) ISE (d) ITSE.**

TABLE 2. **Computational time and magnitude of fault swings.**

Test Case	Controller	Computational Time and Magnitude of swings					
		Computational Time (s)	F1 1st Swing Magnitude t = 0.267 s	F1 2nd Swing Magnitude t = 0.822 s	F1 3rd Swing Magnitude t = 1.53 s	F1 4th Swing Magnitude t =2.23 s	
Case 1	No SDC	16.506916	0.01346	0.001144	0.005574	0.00271	
	ANFTskC	20.908092	0.01346	0.00113	0.004714	0.002139	
	ANFMoWC	22.861283	0.01346	0.001111	0.004442	0.001864	
	ANFMhWC	25.226879	0.01346	0.001131	0.003988	0.001565	
Case 2	No SDC	22.022676	0.001775	0.01898	0.009849	0.00477	
	ANFTskC	32.641962	0.001775	0.01801	0.00841	0.004268	
	ANFMoWC	38.115933	0.001775	0.01794	0.008033	0.003909	
	ANFMhWC	43.418354	0.001775	0.01807	0.007085	0.003005	
					F2 1st Swing Magnitude At t=6.451 s	**F2 2nd Swing Magnitude At t=6.838 s**	**F3 1st Swing Magnitude At t=10.44 s**
Case 3	No SDC	49.253217	0.01858	0.01452	-0.0083	0.006657	-0.008747
	ANFTskC	52.325001	-0.01629	0.0124	-0.007638	0.00557	-0.007624
	ANFMoWC	62.943111	-0.01628	0.0123	-0.007615	0.005529	-0.007623
	ANFMhWC	61.305483	-0.01637	0.01235	-0.007612	0.005176	-0.007622

**F1=fault, F2=fault 2 and F3=fault 3*

to reduce these oscillations and a significant impact of their performance can be seen in the subsequent 3rd, 4th, and 5th swings and then it reached to its steady state.

The percentage performance improvement is shown in Table 3. It shows that the performance is significantly improved by the inclusion of WNN in the consequent part of the network. Thus, depicting a significant improvement margin from ANFTskC to ANFMoWC. The performance margin between proposed controllers was not visible in a steady-state for speed deviation results. However, it is clear from Table 3 that ANFMhWC has shown better performance than ANFMoWC in both transient and steady-state regions.

The percentage performance improvement is much better for multiple faults in the series case. The best ADC performance is achieved in the third case when the test system is subjected under different variations with time like cascade symmetrical and unsymmetrical faults. The ISE and IAE are only using the error signal itself; however, ITSE and ITAE are calculating the performance over time. Thus the later one depicts the improvement in steady-state regions.

In case 1, better performance has been observed in ISE and ITSE and ITAE. This shows that better damping of oscillations has been achieved in the steady-state region. Case 2 depicts a lower performance improvement when compared with other results as the faulted line is removed from the system and again reclosed after the applied fault is cleared. A significant performance margin for all the four PIs has been observed in Case 3. Reason for this is the excellent

TABLE 3. Performance enhancement w.r.t. STATCOM with no ADC [%].

Test Cases	Controller	Performance Index			
		IAE	ISE	ITAE	ITSE
Case 1	ANFTskC	5.32	14.62	5.59	12.28
	ANFMoWC	10.02	26.12	16.44	18.38
	ANFMhWC	16.63	39.67	33.02	24.54
Case 2	ANFTskC	7.36	13.51	7.57	16.39
	ANFMoWC	10.60	15.68	14.61	21.01
	ANFMhWC	16.74	18.17	27.71	27.67
Case 3	ANFTskC	24.08	36.79	27.63	35.56
	ANFMoWC	28.50	39.43	32.99	38.37
	ANFMhWC	34.25	45.72	41.39	43.95

performance of the proposed ANFMhWC and ANFMoWC in both transient and steady-state regions.

V. CONCLUSION

This article demonstrates an NFWC based simulation framework as an ADC for STATCOM. Time-domain analysis has been done for comparative performance evaluation of the proposed control schemes. The obtained results reveal that for multi-machine test systems, the Morlet wavelet based proposed controller ANFMoWC performs consistently better than conventional ANFTskC in damping low frequency modes of oscillations. Furthermore, changing the consequent part from Morlet to advanced Mexican hat base WNN controller (ANFMhWC) improves the performance even more, highlighting WNN's importance in the NeuroFuzzy system. The qualitative and quantitative analysis of performance indices shows that ANFMhWC has the best performance among all controllers. As the remote signals for speed deviations were used for the controller input, assuming that the transmission delays are negligible. This is the only limitation of this approach. In a more practical scenario, the effect of delay can be incorporated, and proposed control is evaluated with the inclusion of transmission delay. The investigation of the integration of wind and solar energy and the impact of STATCOM based damping control on the hybrid grid is a promising future aspect of this research. Although a gradient descent optimization algorithm method was used in this research, advanced optimization algorithms can also be used in the future.

ABBREVIATIONS

STATCOM: Static Synchronous Compensator, VAR: Volt Ampere Reactive, TSK: Takagi-Sugeno-Kang, WNN: Wavelet Neural Network, ANF: Adaptive NeuroFuzzy, MhWC: Mexican hat Wavelet Control, MoWC: Morlet Wavelet Control, PV: Photovoltaic, FACTS: Flexible Alternating Current Transmission System, PSSs: Power System Stabilizers, HSE: Harmony Search Evolutionary, ICA: Imperialist Competitive Algorithm, ADC: Auxiliary Damping Control, PIs: Performance Indices, ANFTskC: Adaptive NeuroFuzzy TSK Control, NN: Neural Network, BP: Back Propagation, STD: Standard Deviation, ITSE: Integral Time Square Error, ITAE: Integral Time Absolute Error, ISE: Integral Square Error, IAE: Integral Absolute Error, FIS: Fuzzy Inference System, ANN: Artificial Neural Network.

REFERENCES

[1] M. A. Basit, S. Dilshad, R. Badar, and S. M. Sami ur Rehman, "Limitations, challenges, and solution approaches in grid-connected renewable energy systems," *Int. J. Energy Res.*, vol. 44, no. 6, pp. 4132–4162, May 2020, doi: 10.1002/er.5033.

[2] P. S. Kundur, *Power System Dynamics and Stability*. New York, NY, USA: McGraw-Hill, 1994.

[3] O. P. Veloza and F. Santamaria, "Analysis of major blackouts from 2003 to 2015: Classification of incidents and review of main causes," *Electr. J.*, vol. 29, no. 7, pp. 42–49, Sep. 2016, doi: 10.1016/j.tej.2016.08.006.

[4] M. A. Abido, "Power system stability enhancement using FACTS controllers: A review," *Arabian J. Sci. Eng.*, vol. 34, no. 1B, pp. 153–172, 2009.

[5] N. Khan, S. Dilshad, R. Khalid, A. R. Kalair, and N. Abas, "Review of energy storage and transportation of energy," *Energy Storage*, vol. 1, no. 3, Jun. 2019, doi: 10.1002/est2.49.

[6] N. Abas, S. Dilshad, A. Khalid, M. S. Saleem, and N. Khan, "Power quality improvement using dynamic voltage restorer," *IEEE Access*, vol. 8, pp. 164325–164339, 2020, doi: 10.1109/ACCESS.2020.3022477.

[7] K. Habur and D. O'Leary, "FACTS-flexible alternating current transmission systems: For cost effective and reliable transmission of electrical energy," Siemens-World Bank Doc. Erlangen, Germany, Draft Rep., 2004, p. 46. [Online]. Available: http://www.academia.edu/download/41305916/facts_siemens.pdf

[8] N. G. Hingorani and L. Gyugyi, *Understanding FACTS: Concepts and Technology of Flexible AC Transmission Systems*. New York, NY, USA: Wiley, 2000.

[9] A. Ganesh, R. Dahiya, and G. K. Singh, "A novel robust STATCOM control scheme for stability enhancement in multimachine power system," *Electron. Electr. Eng.*, vol. 20, no. 4, pp. 22–28, Apr. 2014, doi: 10.5755/j01.eee.20.4.4940.

[10] S. R. Paital, P. K. Ray, and A. Mohanty, "Swarm and BAT algorithm optimized 2DOF-FOPID based STATCOM controller for transient stability enhancement," in *Proc. Prog. Electromagn. Res. Symp.-Fall (PIERS-FALL)*, Nov. 2017, pp. 1961–1968, doi: 10.1109/PIERS-FALL.2017.8293459.

[11] S. Choudhury, A. Satpathy, P. Rout, B. K. Prusty, S. Bhakat, and T. P. Dash, "A robust modified harmony search evolutionary technique for transient stability enhancement in a two machine system through STATCOM," in *Proc. IEEE Int. Conf. Electr., Comput. Commun. Technol. (ICECCT)*, Feb. 2019, pp. 1–8, doi: 10.1109/ICECCT.2019.8869081.

[12] S. M. Abd-Elazim and E. S. Ali, "Imperialist competitive algorithm for optimal STATCOM design in a multimachine power system," *Int. J. Electr. Power Energy Syst.*, vol. 76, pp. 136–146, Mar. 2016, doi: 10.1016/j.ijepes.2015.09.004.

[13] R. Badar and S. Dilshad, "Adaptive Type-2 NeuroFuzzy wavelet-based supplementary damping controls for STATCOM," *Int. Trans. Elect. Energy Syst.*, vol. 30, no. 8, Aug. 2020, Art. no. e12429, doi: 10.1002/2050-7038.12429.

[14] A. Marjanian and E. Jafari, "Transient stability improvement with neuro-fuzzy control of STATCOM in single-machine system," in *Proc. Int. Conf. Energy, Autom. Signal*, Dec. 2011, pp. 1–6, doi: 10.1109/ICEAS.2011.6147209.

[15] G. Shahgholian, E. Mardani, M. Mahdavian, M. Janghorbani, M. Azadeh, and S. Farazpey, "Impact of PSS and STATCOM on dynamic parameters of power system based on neuro-fuzzy controllers," in *Proc. 13th Int. Conf. Electr. Eng./Electron., Comput., Telecommun. Inf. Technol. (ECTI-CON)*, Jun. 2016, pp. 1–6, doi: 10.1109/ECTICon.2016.7561243.

[16] S. Morris, M. A. G. Ezra, and Y. S. Lim, "Multi-machine power transmission system stabilization using MPSO based neuro-fuzzy hybrid controller for STATCOM/BESS," *Int. Rev. Elect. Eng.*, vol. 7, no. 2, pp. 4123–4133, 2012.

[17] R. H. Abiyev and O. Kaynak, "Fuzzy wavelet neural networks for identification and control of dynamic plants—A novel structure and a comparative study," *IEEE Trans. Ind. Electron.*, vol. 55, no. 8, pp. 3133–3140, Aug. 2008, doi: 10.1109/TIE.2008.924018.

[18] Y. Bodyanskiy and O. Vynokurova, "Hybrid adaptive wavelet-neuro-fuzzy system for chaotic time series identification," *Inf. Sci.*, vol. 220, pp. 170–179, Jan. 2013, doi: 10.1016/j.ins.2012.07.044.

[19] T. Q. D. Khoa, L. M. Phuong, P. T. T. Binh, and N. T. H. Lien, "Application of wavelet and neural network to long-term load forecasting," in *Proc. Int. Conf. Power Syst. Technol. (PowerCon)*, Nov. 2004, pp. 840–844, doi: 10.1109/ICPST.2004.1460110.

[20] R. H. Abiyev, "A Type-2 fuzzy wavelet neural network for time series prediction," in *Trends in Applied Intelligent Systems*. Berlin, Germany: Springer, 2010, pp. 518–527.
[21] R. H. Abiyev, "Fuzzy wavelet neural network for prediction of electricity consumption," *Artif. Intell. Eng. Design, Anal. Manuf.*, vol. 23, no. 2, pp. 109–118, May 2009, doi: 10.1017/S0890060409000018.
[22] V. T. Yen, W. Y. Nan, and P. Van Cuong, "Recurrent fuzzy wavelet neural networks based on robust adaptive sliding mode control for industrial robot manipulators," *Neural Comput. Appl.*, vol. 31, no. 11, pp. 6945–6958, Nov. 2019, doi: 10.1007/s00521-018-3520-3.
[23] S. Qamar, U. Khalid, and M. B. Qureshi, "Vehicle suspension control using recurrent neurofuzzy wavelet network," *Vehicle Eng.*, vol. 3, p. 6, 2015. [Online]. Available: https://issuu.com/sep2011--now/docs/ve036_3_0_6_15
[24] M. Tofighi, M. Alizadeh, S. Ganjefar, and M. Alizadeh, "Direct adaptive power system stabilizer design using fuzzy wavelet neural network with self-recurrent consequent part," *Appl. Soft Comput.*, vol. 28, pp. 514–526, Mar. 2015, doi: 10.1016/j.asoc.2014.12.013.
[25] R. Badar and L. Khan, "Adaptive neuro fuzzy wavelet based SSSC damping control paradigm," in *Proc. 10th Int. Conf. Frontiers Inf. Technol.*, Dec. 2012, pp. 101–106, doi: 10.1109/FIT.2012.27.
[26] H. F. Wang, "Phillips–Heffron model of power systems installed with STATCOM and applications," *IEE Proc., Gener., Transmiss. Distrib.*, vol. 146, no. 5, pp. 521–527, 1999, doi: 10.1049/ip-gtd:19990333.
[27] R. Badar and S. Dilshad, "Type-II neuro fuzzy wavelet control for power system stability enhancement using STATCOM," in *Proc. 19th Int. Multi-Topic Conf. (INMIC)*, Dec. 2016, pp. 1–7, doi: 10.1109/INMIC.2016.7840126.
[28] L. A. Zadeh, "Fuzzy sets," *Inf. Control*, vol. 8, no. 3, pp. 338–353, Jun. 1965, doi: 10.1016/S0019-9958(65)90241-X.
[29] R. Babuška and H. Verbruggen, "Neuro-fuzzy methods for nonlinear system identification," *Annu. Rev. Control*, vol. 27, no. 1, pp. 73–85, Jan. 2003, doi: 10.1016/S1367-5788(03)00009-9.
[30] A. Celikyilmaz and I. B. Turksen, *Modeling Uncertainty With Fuzzy Logic?: With Recent Theory and Applications*. Berlin, Germany: Springer, 2009.
[31] M. A. Basit, R. Badar, and F. U. Jan, "Intelligent damping control for transient stability enhancement using HVDC," in *Proc. Int. Conf. Electr. Eng. (ICEE)*, Feb. 2018, pp. 1–6, doi: 10.1109/ICEE.2018.8566770.
[32] G. S. Cheng, "Model-free adaptive control with cybocon," in *Techniques for Adaptive Control*. Amsterdam, The Netherlands: Elsevier, 2003, pp. 145–202.
[33] S. Panda and R. N. Patel, "Improving power system transient stability with an off-centre location of shunt FACTS devices," *J. Elect. Eng.*, vol. 57, no. 6, pp. 365–368, 2006.
[34] M. Tavazoei, "Time response analysis of fractional-order control systems: A survey on recent results," *Fractional Calculus Appl. Anal.*, vol. 17, no. 2, Jan. 2014, doi: 10.2478/s13540-014-0179-z.

SAAD DILSHAD (Graduate Student Member, IEEE) received the B.Sc. degree in electrical engineering from the University of Gujrat, Pakistan, in 2013, and the M.S. degree in electrical engineering from COMSATS University Islamabad, Islamabad, Pakistan, in 2017, where he is currently pursuing the Ph.D. degree in solar thermal cooling system using CO_2 as refrigerant. He received the HEC Indigenous Scholarship for M.S. leading to Ph.D. by HEC, Pakistan. He has published 11 publications in well reputed International Journals and IEEE international conferences. He also received the U.S.–Pak Startup and Ideation Training by RTI Internationals, USA, in 2018. His research interests include NeuroFuzzy systems, soft computing, power system stability, FACTS devices, HVDC systems, fuel cell, energy storage systems, natural refrigerants, solar thermal systems, CO_2 refrigeration, and renewable energy integration with FACTS devices.

NAEEM ABAS (Member, IEEE) received the Ph.D. degree in electrical engineering from the COMSATS Institute of Information Technology, Islamabad. He has done the Ph.D. research work on solar thermal water heating system at North Dakota State University, Fargo, ND, USA, as a Research Associate.

He is currently an Associate Professor with the Department of Electrical Engineering, University of Gujrat, Hafiz Hayat campus. He is also a keen researcher in electrical and energy engineering, environmental systems, solar thermal systems, and harmonic analysis. He has published 45 research articles in ISI Indexed IF Journals, 9 articles in International Journals, 1 U.S. patent, 4 International Book chapters, and more than 30 International Conference articles.

HAROON FAROOQ (Member, IEEE) received the Ph.D. degree in electrical engineering from Glasgow Caledonian University, U.K., in 2012. He is currently an Assistant Professor with the Electrical Engineering Department (RCET, Gujranwala), University of Engineering and Technology at Lahore, Lahore, Pakistan. His research interests include power quality, renewable energy systems, electric vehicles, and demand side management.

ALI RAZA KALAIR received the B.Sc. degree in electrical engineering from Air University Islamabad and the M.S. degree in electrical engineering from COMSATS University Islamabad, Pakistan. He is currently pursuing the Ph.D. degree in electrical engineering with the Department of Telecommunications, Electrical, Robotics and Biomedical Engineering, Swinburne University, Australia. He has published more than ten impact factor articles in reputed journals. His research interests include renewable energy systems, solar cooling, and power system harmonics & filter design.

AWAIS AHMED MEMON received the B.E. degree in electrical engineering from the Quaid-e-Awam University of Engineering & Technology (QUEST), Nawabshah, in 2006. He is currently pursuing the M.S. degree in electrical engineering with the University of Gujrat, Gujrat. In 2007, he joined as an Electrical Engineer with Zaver Pearl Continental Hotel, Gwadar. In 2008, he joined as a Junior Engineer with Gujranwala Electric Power Company (GEPCO), Gujranwala, a power distribution company. During his service, he has undergone different technical and management trainings. He is a Registered Member of the Pakistan Engineering Council. He is currently an Additional Executive Engineer with GEPCO. He is an active researcher in field of power engineering, and power system stability and control.